

Finding novelty with uncertainty

Jacob C. Reinhold^a, Yufan He^a, Shizhong Han^b, Yunqiang Chen^b, Dashan Gao^b, Junghoon Lee^c,
Jerry L. Prince^{a,d}, and Aaron Carass^{a,d}

^aDepartment of Electrical and Computer Engineering, Johns Hopkins University,
Baltimore, MD, USA 21218

^b12 Sigma Technologies, San Diego, CA USA 92122

^cDepartment of Radiation Oncology, Johns Hopkins School of Medicine,
Baltimore, MD, USA 21287

^dDepartment of Computer Science, Johns Hopkins University, Baltimore, MD, USA 21218

ABSTRACT

Medical images are often used to detect and characterize pathology and disease; however, automatically identifying and segmenting pathology in medical images is challenging because the appearance of pathology across diseases varies widely. To address this challenge, we propose a Bayesian deep learning method that learns to translate healthy computed tomography images to magnetic resonance images and simultaneously calculates voxel-wise uncertainty. Since high uncertainty occurs in pathological regions of the image, this uncertainty can be used for unsupervised anomaly segmentation. We show encouraging experimental results on an unsupervised anomaly segmentation task by combining two types of uncertainty into a novel quantity we call *scibilic* uncertainty.

Keywords: Unsupervised anomaly segmentation, image translation, uncertainty quantification

1. INTRODUCTION

When pathology is present in structural medical images, such as computed tomography (CT) and magnetic resonance (MR), machine learning methods can be used to segment the specific pathology;¹ however, reliable machine learning-based segmentation currently requires a labeled dataset of that pathology. But labeled datasets do not exist for all diseases, so having a machine learning method that does not rely on pathology-specific labels is desirable. In this paper, we propose a novel, simple-to-implement method of unsupervised anomaly segmentation that uses estimates of *epistemic* and *aleatoric* uncertainty² to find anomalies (i.e., novelty) in medical images. Our method is competitive with state-of-the-art methods.

The goal of unsupervised anomaly segmentation is to use unlabeled data (i.e., data without ground-truth segmentation labels) to train a model that automatically segments anomalous regions of a new image. Generally, prior methods have relied on training either an autoencoder^{3,4} or a generative adversarial network⁵⁻⁷ on only healthy data and using the voxel-wise reconstruction error as a heatmap for anomaly segmentation.⁸ The underlying principle is: since the network has only ever seen healthy data, reconstruction will be poor in regions of anomaly. However, unsupervised anomaly segmentation relying on reconstruction error perform poorly, motivating the need for alternative approaches.

Uncertainty estimation in deep neural networks (DNN) for image translation, segmentation, and super-resolution has been explored;⁹⁻¹¹ however, in this work, we use the uncertainty estimates to do unsupervised anomaly segmentation. While a limited version of this has been explored by Pawlowski et al.,¹² we introduce a novel combination of uncertainty measures to increase the detection rate of anomalies as well as improve anomaly segmentation.

To estimate uncertainty, we used the work of Gal and Ghahramani¹³ who showed that dropout¹⁴ can be used to learn an approximate distribution over the weights of a DNN—a form of Bayesian inference. Then,

Further author information: (Send correspondence to J.C.R.)

J.C.R.: E-mail: jacob.reinhold@jhu.edu

during prediction, dropout is used in a Monte Carlo framework to draw weights from this fitted approximate distribution. The sample variance of the output from several stochastic forward passes corresponds to uncertainty about what the model knows (*epistemic* uncertainty). We also modified the network architecture to create an additional output that corresponds to a variance parameter, which is fit by changing the loss function;¹⁵ this corresponds to the uncertainty about the measurement quality (*aleatoric* uncertainty).

We modified a state-of-the-art supervised image translation DNN—a U-Net¹—to capture both types of uncertainty in a CT-to-MR image translation task. The CT-to-MR task is explored here because CT is far more common than MR images, but soft tissue anomalies are harder to detect in CT images. The underlying principle proposed in this paper, however, should apply broadly to reconstruction or synthesis tasks; it is not specific to the CT-to-MR synthesis task. We show that our modified U-Net produces uncertainty estimates that can be used to competitively detect and segment anomalies through a combined quantity we call *sciblic* uncertainty.

2. METHODS

In this section, we describe 1) the relevant uncertainty estimation theory and 2) our modifications to a U-Net to estimate uncertainty.

2.1 Uncertainty estimation

Following the work of Gal,¹⁶ we used the variance of the prediction as a proxy for predictive uncertainty. Predictive uncertainty can be split into two discrete, interpretable forms which separately estimate epistemic and aleatoric uncertainty. In the following paragraphs we will mathematically define the predictive uncertainty from which epistemic and aleatoric uncertainty are derived.

Let our training data be denoted as $\mathcal{D} = \{(\mathbf{x}_i, \mathbf{y}_i) \mid \mathbf{x}_i, \mathbf{y}_i \in \mathbb{R}^M, i \in \{1, 2, \dots, N\}\}$, where each $(\mathbf{x}_i, \mathbf{y}_i)$ pair are images—co-registered MR and CT images, in our case—of flattened length M . Our goal was to fit the predictive distribution,

$$p(\mathbf{y}^* \mid \mathbf{x}^*, \mathcal{D}) = \int p(\mathbf{y}^* \mid \mathbf{x}^*, \mathbf{W}) p(\mathbf{W} \mid \mathcal{D}) d\mathbf{W}, \quad (1)$$

where $(\mathbf{x}^*, \mathbf{y}^*) \notin \mathcal{D}$ is test data and \mathbf{W} are the weights of a (multi-task) neural network $f^{\mathbf{W}}(\cdot)$. The fitted predictive distribution gave us estimates of the predictive mean and variance, which are the synthesized image and predictive uncertainty, respectively.

To obtain the predictive distribution, however, we needed to estimate the posterior $p(\mathbf{W} \mid \mathcal{D})$. This posterior probability distribution over the weights allows us to determine epistemic uncertainty, since we expect the model to produce consistent outputs for known regions (i.e., low sample variance) and inconsistent outputs for unknown regions (i.e., high sample variance). But estimating the posterior distribution is not feasible due to the intractable integral implicit in the denominator after applying Bayes rule.

To avoid this problem, we used variational inference¹⁷ to fit an approximate distribution, $q_\theta(\mathbf{W})$, to $p(\mathbf{W} \mid \mathcal{D})$ via optimization. The approximate distribution was fit by minimizing the Kullback-Leibler (KL) divergence between $q_\theta(\mathbf{W})$ and $p(\mathbf{W} \mid \mathcal{D})$ using the work of Gal and Ghahramani.¹³ They showed that using dropout on the full set of weights of the DNN, θ , during normal DNN training minimizes $\text{KL}(q_\theta(\mathbf{W}) \parallel p(\mathbf{W} \mid \mathcal{D}))$. We used this method of variational inference to get $q_\theta^*(\mathbf{W})$, the *fitted* approximate distribution. We then sampled the model weights, $\widehat{\mathbf{W}} \sim q_\theta^*(\mathbf{W})$, to estimate the predictive distribution, i.e., $q_\theta^*(\mathbf{W})$ replaced $p(\mathbf{W} \mid \mathcal{D})$ in Eq. (1).

To find a voxel-wise estimate of aleatoric uncertainty, we assumed the likelihood has the following form,

$$p(\mathbf{y} \mid \mathbf{x}, \mathbf{W}) = \mathcal{N}(\mathbf{y}; \hat{\mathbf{y}}, \text{diag}(\hat{\boldsymbol{\sigma}})^2), \quad (2)$$

where $\hat{\mathbf{y}} = f_{\hat{\mathbf{y}}}^{\mathbf{W}}(\mathbf{x})$ and $\hat{\boldsymbol{\sigma}}^2 = f_{\hat{\boldsymbol{\sigma}}^2}^{\mathbf{W}}(\mathbf{x})$ are each outputs of our multi-task neural network. Taking the negative logarithm of Eq. (2) results in a modified form of the mean square error for the loss function,

$$\mathcal{L}(\mathbf{y}, \hat{\mathbf{y}}) = \frac{1}{M} \sum_{i=1}^M \frac{1}{2} \hat{\sigma}_i^{-2} \|\mathbf{y}_i - \hat{\mathbf{y}}_i\|_2^2 + \frac{1}{2} \log \hat{\sigma}_i^2. \quad (3)$$

When we learn the weights of the DNN according to Eq. (3), we are doing maximum likelihood estimation not only for $\hat{\mathbf{y}}$, but for the parameter $\hat{\sigma}^2$, which is a voxel-wise estimate of the data variance—a quantity related to aleatoric uncertainty.

As a result of these assumptions and problem setup, we can approximate the predictive variance of a test sample as follows:

$$\text{Var}(\mathbf{y}^*) \approx \underbrace{\frac{1}{T} \sum_{t=1}^T \text{diag}(f_{\hat{\sigma}^2}^{\mathbf{W}_t}(\mathbf{x}^*))}_{\text{aleatoric}} + \underbrace{\frac{1}{T} \sum_{t=1}^T f_{\hat{\mathbf{y}}}^{\mathbf{W}_t}(\mathbf{x}^*) f_{\hat{\mathbf{y}}}^{\mathbf{W}_t}(\mathbf{x}^*)^\top - \left(\frac{1}{T} \sum_{t=1}^T f_{\hat{\mathbf{y}}}^{\mathbf{W}_t}(\mathbf{x}^*) \right) \left(\frac{1}{T} \sum_{t=1}^T f_{\hat{\mathbf{y}}}^{\mathbf{W}_t}(\mathbf{x}^*) \right)^\top}_{\text{epistemic}},$$

where T is the number of sampled weights. Consequently, the epistemic uncertainty is the term in the predictive variance that corresponds to sample variance while the aleatoric uncertainty is the term associated with the estimated variance of the data.

To create a heatmap used to detect anomalies, we then divided the epistemic uncertainty by the aleatoric uncertainty term at every voxel. The result captures pathologies because a DNN trained only on healthy data should exhibit high epistemic uncertainty in the region of a pathology; but areas of high aleatoric uncertainty may also have high epistemic uncertainty simply due to the network not being able to reliably estimate the corresponding regions (resulting from intrinsic properties of the data). The voxel-wise division retains areas of high epistemic uncertainty while reducing the intensity of regions where the model just performs poorly. We can then use simple thresholding on the quotient to detect anomalies in test data. We call this novel quantity *scibilic*^{*} uncertainty because it highlights the areas the model could know how to predict—provided sufficient representative training data—but does not.

2.2 Network architecture

We used a U-Net¹ architecture modified as follows:

- We used two 3D convolutional layers, one at the start and one at the end. This improved sharpness and slice-to-slice consistency.
- We downsampled and upsampled three times instead of four. Experimental results showed no improvement with four downsample operations.
- We substituted max-pooling layers for strided convolutions in downsampling. For upsampling we used nearest-neighbor interpolation followed by a 5^2 convolution.¹⁸
- We attached two heads to the end of the network, where one output $\hat{\mathbf{y}}$ and the other output $\hat{\sigma}^2$. Both consisted of 3^3 and 1^3 convolutional layers.
- We concatenated the input image to the feature maps output by the network immediately before both heads.¹⁹
- We used spatial dropout²⁰ ($p = 0.2$) on all layers except the heads, because it drops weights on convolutional layers unlike standard dropout.¹⁴
- We used the AdamW optimizer²¹ with weight decay 10^{-6} , learning rate 0.003, $\beta = (0.9, 0.99)$, and batch size 36.
- We used $T = 50$ weight samples in prediction.

3. RESULTS

3.1 Dataset

We used non-contrast T_1 -w and CT images from 51 subjects on a protocol for retrospective data analysis approved by the institutional review board. Fifty of the subjects were considered to be healthy, and the remaining subject had anomalies in the brain and was excluded from training and validation. The T_1 -w images were acquired on a Siemens Magnetom Espree 1.5T scanner (Siemens Medical Solutions, Erlangen, Germany, TE = 4.24 ms,

^{*}*Scibilic* is an anglicized version of the Latin adjective *scibilis*, which means knowable.

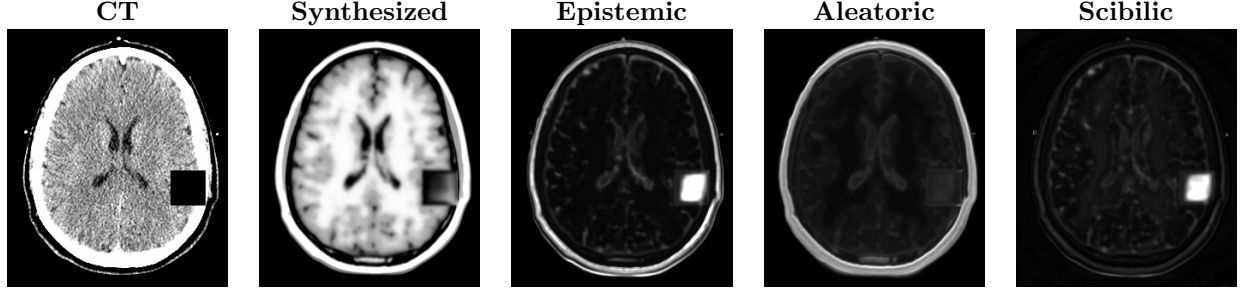


Figure 1. **Synthetic anomaly:** Shown is an example synthetic anomaly CT image and the corresponding estimated T_1 -w image, epistemic, aleatoric, and scibilic (epistemic / aleatoric) uncertainty.

TR = 1130 ms, flip angle = 15° , image size = 512×512 pixels, pixel size = 0.5×0.5 mm², slice thickness = 1 mm); geometric distortions were corrected on the Siemens Syngo application. All T_1 -w images were processed to normalize the white matter mean.²² The CT images were acquired on a Philips Brilliance Big Bore scanner (Philips Medical Systems, Andover, MA, image size = 512×512 pixels, pixel size = 0.6×0.6 mm² 0.8×0.8 mm², slice thickness = 1.0 mm). All images were resampled to have a digital resolution of $0.7 \times 0.7 \times 1.0$ mm³. Finally, the T_1 -w images were rigidly registered to the CT images. For training, the T_1 -w and CT images were split into overlapping $128 \times 128 \times 8$ patches. We used 45 of the healthy subjects for training and the remaining five healthy subjects for validation. Test images were split into three overlapping segments along the inferior-superior axis due to memory constraints.

3.2 Unsupervised anomaly segmentation

In our first experiment, we inserted synthetic anomalies into otherwise healthy data—the five held-out validation datasets—and calculated the resulting Dice coefficient²³ and detection rate over a range of thresholds. Our synthetic anomaly is an all-zero cube, of side-length 40 voxels, placed randomly inside the brain mask of the five held-out healthy CT images (see Fig. 1 for an example). We created five of these anomalies per test subject by varying anomaly location. These 25 synthetic anomalous data were used as input to the trained network. Quantitative results are in Fig. 2, where Intersection over Union (IoU) is used to indicate detection according to several IoU thresholds. Specifically, we calculated the IoU—also known as Jaccard index²⁴—for the largest-connected component of the binary prediction thresholded at 0.15.

In our second experiment, we tested the trained network on the held-out pathological dataset (pathology in

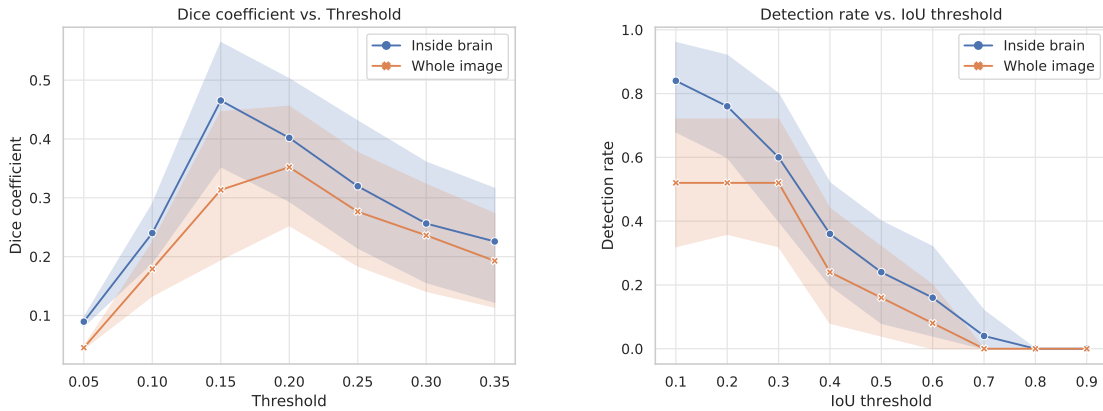


Figure 2. **Dice coefficient on synthetic anomalies:** Shown are the Dice coefficients (left) and detection rate (right) calculated on the 25 test images. The threshold in the Dice coefficient plot corresponds to the binarization threshold. The IoU threshold in the detection rate plot corresponds to the IoU threshold used to determine detection. Shaded regions are bootstrapped 95% confidence intervals.

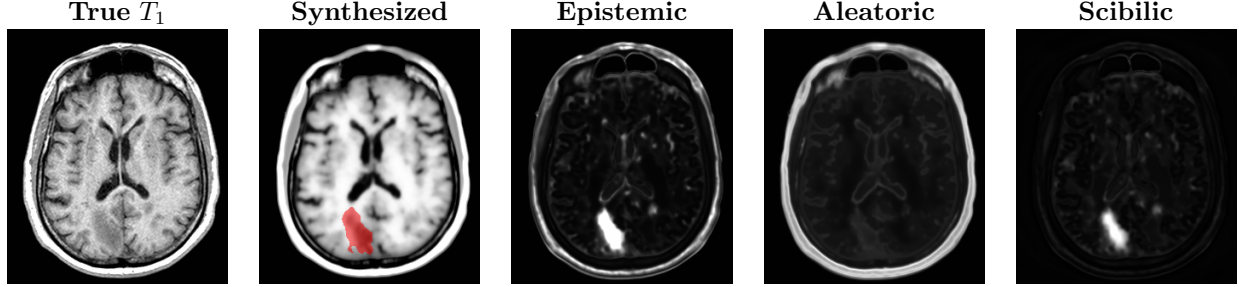


Figure 3. **Example anomalous image:** Shown is an example anomalous image and corresponding synthesized image along with the estimated epistemic and aleatoric uncertainty maps as well as their voxel-wise quotient (scibilic). The red overlay in the synthesized image is the largest-connected component of the binarized scibilic uncertainty image at a threshold of 0.15, which was the optimal threshold in the synthetic anomaly experiment.

the occipital lobe) collected on the same scanner. Since we do not have a ground-truth label for this data set we show qualitative results in Fig. 3.

4. DISCUSSION AND CONCLUSION

Detecting and segmenting pathologies in structural medical images is difficult, especially without labels. In the experiments above, we showed that measures of uncertainty can be used to highlight anomalous regions in images simply by training the proposed network on healthy data alone. Importantly, this anomalous region segmentation is done in conjunction with a CT-to-MR image translation task that provides more insight into the fine anatomical structures of the subject. While the resulting synthesized image is not state-of-the-art, the additional information provided by the estimates of uncertainty provides researchers with a greater ability to understand the model and data as well as detect and segment anomalies in test images.

ACKNOWLEDGMENTS

This work was supported by 12 Sigma Technologies.

REFERENCES

- [1] Ronneberger, O., Fischer, P., and Brox, T., “U-Net: Convolutional networks for biomedical image segmentation,” in *[International Conference on Medical image computing and computer-assisted intervention]*, 234–241, Springer (2015).
- [2] Der Kiureghian, A. and Ditlevsen, O., “Aleatory or epistemic? does it matter?,” *Structural Safety* **31**(2), 105–112 (2009).
- [3] Zimmerer, D., Kohl, S. A., Petersen, J., Isensee, F., and Maier-Hein, K. H., “Context-encoding variational autoencoder for unsupervised anomaly detection,” *arXiv preprint arXiv:1812.05941* (2018).
- [4] Uzunova, H., Schultz, S., Handels, H., and Ehrhardt, J., “Unsupervised pathology detection in medical images using conditional variational autoencoders,” *International journal of computer assisted radiology and surgery* **14**(3), 451–461 (2019).
- [5] Goodfellow, I., Pouget-Abadie, J., Mirza, M., Xu, B., Warde-Farley, D., Ozair, S., Courville, A., and Bengio, Y., “Generative adversarial nets,” in *[Advances in neural information processing systems]*, 2672–2680 (2014).
- [6] Schlegl, T., Seeböck, P., Waldstein, S. M., Schmidt-Erfurth, U., and Langs, G., “Unsupervised anomaly detection with generative adversarial networks to guide marker discovery,” in *[International Conference on Information Processing in Medical Imaging]*, 146–157, Springer (2017).
- [7] Baur, C., Wiestler, B., Albarqouni, S., and Navab, N., “Deep autoencoding models for unsupervised anomaly segmentation in brain MR images,” in *[International MICCAI Brainlesion Workshop]*, 161–169, Springer (2018).
- [8] An, J. and Cho, S., “Variational autoencoder based anomaly detection using reconstruction probability,” *Special Lecture on IE* **2**, 1–18 (2015).

- [9] Bragman, F. J., Tanno, R., Eaton-Rosen, Z., Li, W., Hawkes, D. J., Ourselin, S., Alexander, D. C., McClelland, J. R., and Cardoso, M. J., “Uncertainty in multitask learning: joint representations for probabilistic MR-only radiotherapy planning,” in [*International Conference on Medical Image Computing and Computer-Assisted Intervention*], 3–11, Springer (2018).
- [10] Nair, T., Precup, D., Arnold, D. L., and Arbel, T., “Exploring uncertainty measures in deep networks for multiple sclerosis lesion detection and segmentation,” in [*International Conference on Medical Image Computing and Computer-Assisted Intervention*], 655–663, Springer (2018).
- [11] Tanno, R., Worrall, D., Kaden, E., Ghosh, A., Grussu, F., Bizzi, A., Sotiropoulos, S. N., Criminisi, A., and Alexander, D. C., “Uncertainty quantification in deep learning for safer neuroimage enhancement,” *arXiv preprint arXiv:1907.13418* (2019).
- [12] Pawlowski, N., Lee, M. C., Rajchl, M., McDonagh, S., Ferrante, E., Kamnitsas, K., Cooke, S., Stevenson, S., Khetani, A., Newman, T., et al., “Unsupervised lesion detection in brain CT using bayesian convolutional autoencoders,” (2018).
- [13] Gal, Y. and Ghahramani, Z., “Dropout as a bayesian approximation: Representing model uncertainty in deep learning,” in [*International conference on machine learning*], 1050–1059 (2016).
- [14] Srivastava, N., Hinton, G., Krizhevsky, A., Sutskever, I., and Salakhutdinov, R., “Dropout: a simple way to prevent neural networks from overfitting,” *The Journal of Machine Learning Research* **15**(1), 1929–1958 (2014).
- [15] Kendall, A. and Gal, Y., “What uncertainties do we need in bayesian deep learning for computer vision?,” in [*Advances in neural information processing systems*], 5574–5584 (2017).
- [16] Gal, Y., *Uncertainty in deep learning*, PhD thesis, University of Cambridge (2016).
- [17] Jordan, M. I., Ghahramani, Z., Jaakkola, T. S., and Saul, L. K., “An introduction to variational methods for graphical models,” *Machine learning* **37**(2), 183–233 (1999).
- [18] Odena, A., Dumoulin, V., and Olah, C., “Deconvolution and checkerboard artifacts,” *Distill* (2016).
- [19] Zhao, C., Carass, A., Lee, J., He, Y., and Prince, J. L., “Whole brain segmentation and labeling from CT using synthetic MR images,” in [*International Workshop on Machine Learning in Medical Imaging*], 291–298, Springer (2017).
- [20] Tompson, J., Goroshin, R., Jain, A., LeCun, Y., and Bregler, C., “Efficient object localization using convolutional networks,” in [*Proceedings of the IEEE Conference on Computer Vision and Pattern Recognition*], 648–656 (2015).
- [21] Loshchilov, I. and Hutter, F., “Decoupled weight decay regularization,” in [*International Conference on Learning Representations*], (2019).
- [22] Reinhold, J. C., Dewey, B. E., Carass, A., and Prince, J. L., “Evaluating the impact of intensity normalization on MR image synthesis,” in [*Medical Imaging 2019: Image Processing*], **10949**, 109493H, International Society for Optics and Photonics (2019).
- [23] Dice, L. R., “Measures of the amount of ecologic association between species,” *Ecology* **26**(3), 297–302 (1945).
- [24] Jaccard, P., “The distribution of the flora in the alpine zone.,” *New phytologist* **11**(2), 37–50 (1912).